ARTICLES
PUBLISHED ONLINE: 25 APRIL 2017 | DOI: 10.1038/NGEO2938
nature geoscience

Groundwater salinity influenced by Holocene seawater trapped in incised valleys in the Red River delta plain

Flemming Larsen[1]*, Long Vu Tran[2], Hoan Van Hoang[2], Luu Thi Tran[3], Anders Vest Christiansen[4] and Nhan Quy Pham[5]

Salty and brackish groundwater has been observed at least 100 km inland in some aquifers contained within Quaternary delta plains. This phenomenon limits access to fresh groundwater resources, particularly in the densely populated deltas of Southeast Asia. However, the causes of inland salinity are unclear. Here we present borehole and geophysical data that show that in the Red River delta plain of Vietnam, salty and brackish groundwater primarily occurs in incised valleys that were formed during sea-level lowstands during the Pleistocene. During the mid-Holocene, these valleys were filled with fine-grained marine deposits containing trapped seawater. We conduct groundwater flow simulations that show that the age, thickness, and permeability of the marine sediments are the primary controls on the leaching of salty porewater into the freshwater aquifer. We find that salty groundwater originating from this trapped seawater is still present in Holocene-aged sediments with low permeability, and affects groundwater salinity in adjacent aquifers. In contrast, trapped seawater from all Pleistocene-aged sediments has been leached. We identify a number of brackish to saline delta aquifers elsewhere in Asia and throughout the world that have a similar sedimentary history, and thus are likely to be influenced by this leaching process.

The coastal zone can be defined to encompass the continental shelf (water depth <200 m), and the adjacent 100 km of land from the coastline[1], which hosts an estimated 20–40% of the global population and 20 of the world's 33 megacities[1,2]. The stresses on water resources in the densely populated coastal zones are thus high, and are likely to be compounded by future sea-level rise, although the impact of this on the groundwater resource is still debated[3]. Groundwater constitutes a significant proportion of the water resources in the coastal zone, but is frequently salty or brackish due to mixing with recent or palaeo-seawater[4]. Therefore, a better hydrogeological understanding of the processes controlling the distribution of fresh, brackish and saltwater in the coastal zone is warranted for the utilization of deltaic water resources.

Processes resulting in high-salinity groundwater in coastal aquifers are: recent natural or pumped induced saltwater intrusion[5–7], salinization due to intrusion from rivers by surface–groundwater interactions[8–11] and the occurrence of palaeo-saltwater, generated under climatic and hydraulic conditions prevailing during the Quaternary period[12].

The ~100 kyr Milankovitch cycles have during the Quaternary period generated large ice caps on continents and led to a sea-level lowerings of 120 to 140 m below the present level[13,14]. These sea-level lowerings have caused the erosion of valley structures into Pleistocene delta plain sediments[15], which during Holocene transgressions were filled up with marine sediments[16,17]. The valley-fill sediments tend to constitute aquifers when they are coarse-grained[16], and aquitards with salty porewater when they are fine-grained and low permeability[18].

Based on a study including 36 deltas worldwide, a deceleration in the sea-level rise between 8.5 and 6.5 kyr ago (ka) has been suggested as a controlling mechanism for the development of Holocene deltas[19]. During delta-front progradation, sedimentation is dominated by coarse-grained fluvial deposits, whereas during transgressions, fine-grained marine sediments, dominated by clays, silts and fine sands rich in organic material, are deposited. In a hydrogeological perspective, this geologic scenario leads to the formation of multi-aquifer systems, with high-permeability alluvial and fluvial deposits forming aquifers and low-permeability marine and fluvial overbank deposits forming interlayered aquitards.

We have conducted a study focused on the geologic, climatic and hydraulic controls of the occurrence of salty groundwater in the Red River delta plain (RRDP) in Vietnam, and similar cases reported in the literature suggest that our findings have implications for understanding the distribution of saline groundwater in Quaternary delta systems worldwide.

The geology of Quaternary deltas and the RRDP

The geology of Quaternary deltas generally consists of coarse-grained Pleistocene, fluvial deposits and more fine-grained, Holocene deposits[19], and the studied RRDP conforms to this model (Fig. 1a), with three sedimentary sequences of Pleistocene age and two of Holocene age[20]. A generalized nortwest–southeast oriented geologic cross-section of the RRDP sediments is depicted in Fig. 2a. The thickness of the Quaternary deposits in the RRDP ranges from a few metres at the flood-plain apex in the northwest to 150–200 m at the coastline in the southeast (Fig. 2a). Coarse-grained clastic alluvial and fluvial deposits were deposited during low sea-level stands in the Pleistocene and 60–80-m-deep valleys were subsequently eroded in these deposits during the latest Pleistocene lowstand (Fig. 1b). Two major incised valley systems have been

[1]Geological Survey of Denmark and Greenland, Øster Voldgade 10, DK-1350 Copenhagen, Denmark. [2]Hanoi University of Mining and Geology, Department of Hydrogeology, Hanoi, Vietnam. [3]Hanoi University of Science, Department of Geology, Hanoi, Vietnam. [4]Department of Geoscience, Aarhus University, Høegh-Guldbergs Gade 2, 8000 Aarhus, Denmark. [5]Hanoi University of Natural Resources and Environment, Hanoi, Vietnam. *e-mail: flar@geus.dk

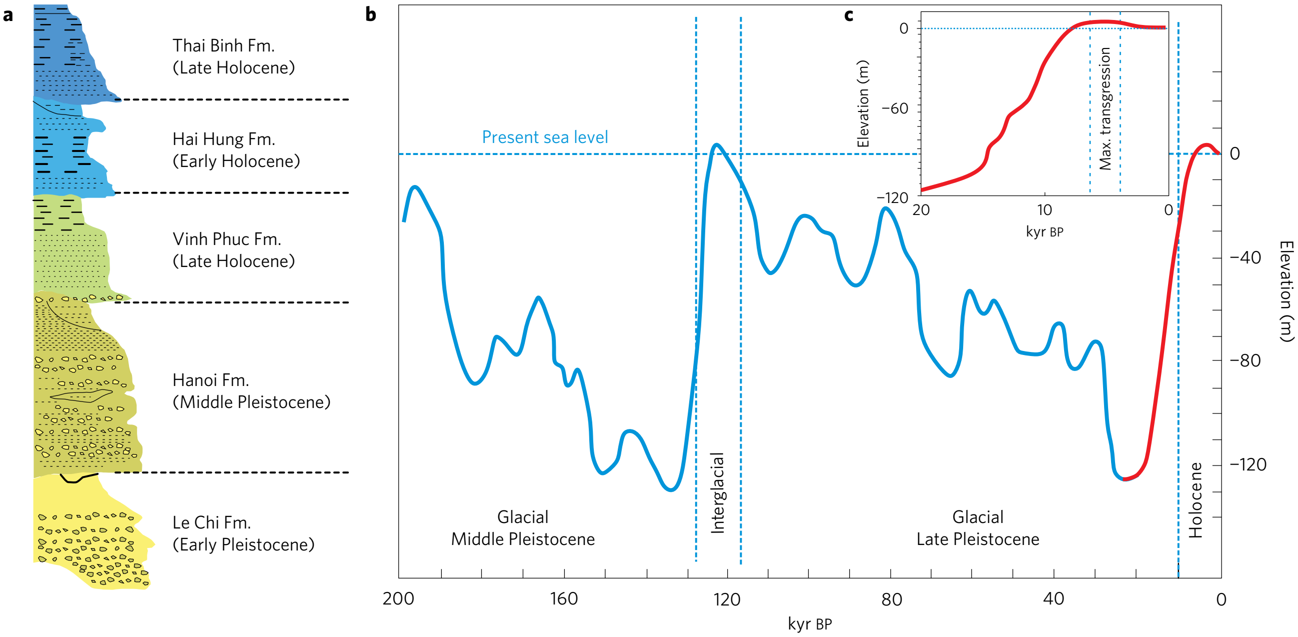

Figure 1 | The Quaternary geology of the RRDP. a, The Quaternary sediment column and formations of the RRDP[18]. **b**, The global eustatic sea-level curve during the past 200 kyr (ref. 14). **c**, The compiled eustatic sea-level curve for the western margin of the South China Sea during the past 20 kyr (ref. 17). Fm., formation.

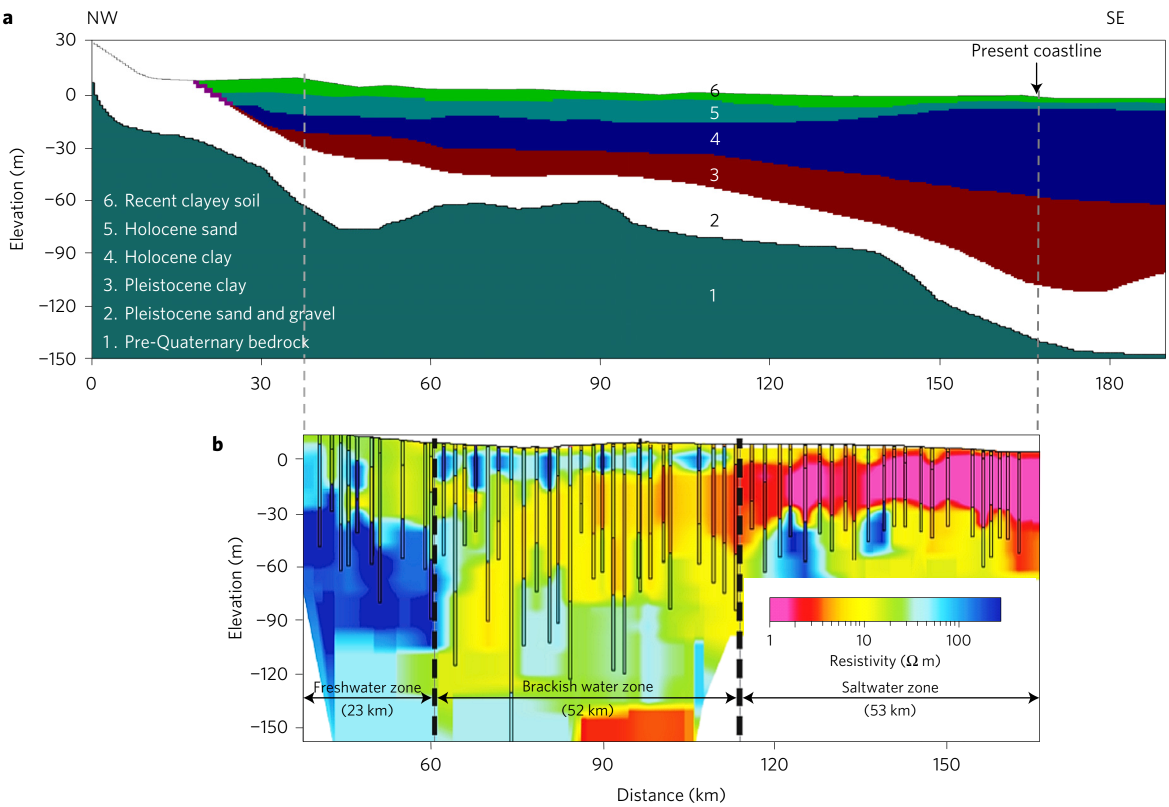

Figure 2 | Subsurface geology and groundwater types based on TEM soundings. a, The geology of the RRDP in the incised valley south of the present Red River. **b**, Inverted earth resistivity models of measured TEM soundings in a geophysical profile line along the shown geologic cross-section. For the locations of the cross-sections, see Fig. 3.

identified in the RRDP, representing a pre-Red River and the more northerly pre-Luoc River, eroded into the coarse-grained fluvial Pleistocene deposits[17,18]. The locations of these two former rivers are indicated by the presence of brackish water in the Pleistocene aquifer today (Fig. 3a). During the Holocene high sea-level stand (Fig. 1b), these valley systems were filled up with fine-grained marine deposits[17]. A more detailed description of the RRDP is given in the Supplementary Information.

Saltwater in the RRDP and Quaternary deltas

In the RRDP Pleistocene aquifer, brackish groundwater is present up to 80 km inland below the two incised valley systems (Fig. 3a).

NATURE GEOSCIENCE DOI: 10.1038/NGEO2938

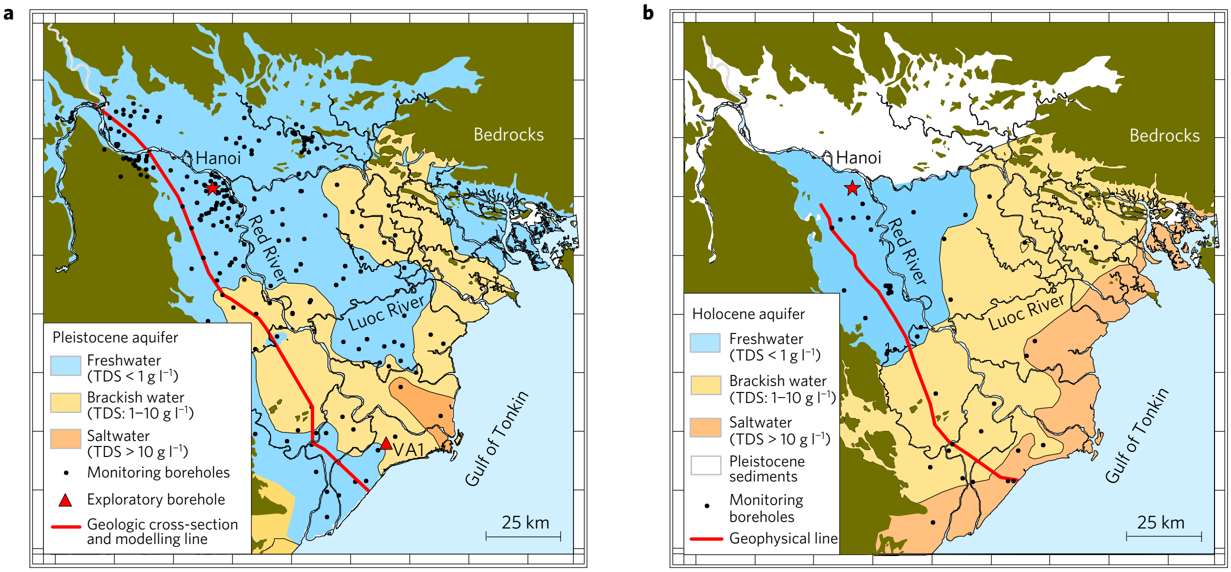

Figure 3 | Saltwater and freshwater in RRDP aquifers. a, The distribution of freshwater, brackish water and saltwater in boreholes drilled into the Pleistocene aquifers. The red line indicates the location of the geologic profile (Fig. 2a) and the numerical simulation section (Fig. 5). **b**, The distribution of freshwater, brackish water and saltwater in boreholes drilled into the Holocene aquifers. The red line indicates the location of the geophysical soundings with TEM measurements (Fig. 2b). TDS, total dissolved solids.

In the shallow Holocene aquifers, brackish groundwater is present as far as 75 km from the coastline, and saltwater up to 25 km from the sea (Fig. 3b). Borehole drilling and a transient electromagnetic sounding (TEM) survey revealed that the incised valleys located in the southwestern is filled with up to 80 m of Holocene marine sediments, dominated by fine-sand, silt and clay (Fig. 2a)[17,18]. Three distinct zones were seen in the geophysical survey (Fig. 2b). The first zone is a landward section (23 km), to the left in Fig. 2b, with a near-surface confining clay layer overlying Holocene, Pleistocene and Neogene sandstone and older limestone, all containing freshwater. The second zone is a central section (52 km) dominated by brackish groundwater. The hydrogeological interpretation suggests an uppermost 1–3-m-thick unit with confining clay layer formed by marine terraces containing brackish porewater. A second high-resistivity layer with a thickness up to 15 m represents regional Holocene unconfined and confined aquifers in sandy deposits with freshwater. A third low-resistivity layer with brackish water in Holocene deposits, down to elevation −80 m, and a fourth lowermost layer which is interpreted as representing a deep Pleistocene aquifer with brackish water. The third zone is a seaward section (53 km), to the right in Fig. 2b, shows predominantly very low electrical resistivity layers down to −30 and −40 m (Fig. 2b). The hydrogeological interpretation of the TEM soundings in this section suggests uppermost confining clays with salty porewater, but areas with fresh, shallow groundwater are locally present. The higher resistivities in layers below are representing Pleistocene gravel and sand with brackish water. A more detailed description of the distribution of salty groundwater in the RRDP is given in the Supplementary Information.

Palaeo-saltwater has been observed at distances up to several hundred km from present coastlines in other Quaternary delta systems, with the most inland occurrence of 300 km in Bangladesh (Table 1). Reported groundwater salinities are as high as 19,600 mg l^{-1} of chloride, which is the concentration in modern seawater. Reported concentrations above 19,600 mg l^{-1} in Table 1 must be explained with evaporation of seawater.

Table 1 | Quaternary delta systems, or coastal aquifers, in which palaeo-saltwater have been reported.

Delta/coastal aquifer	Country	Distance from coastline, km	Max. Cl, g l^{-1}
Red River delta	Vietnam	75	19.6
Pearl River delta	China	60	14.1
Hangzhou river/delta	China	>10?	?
Hamasato aquifer	**Japan**	?	1.0
Bangkok delta	**Thailand**	30	11
Kelantan	**Malaysia**	6	3.6
Jakata	**Indonesia**	?	?
Tista	Bangladesh	300	0.5
Mahanadi	India	17	5.7
Inhaca coastal aquifer	Mozambique	?	?
Coastal basin	Togo	25	0.2
Nile	Egypt	60	13.0
Llobregat	Spain	12	19.6
Dõnana	Spain	18	14.8
Rhone	France	23	19.2
Ferrara	Italy	14	~100
Caen coastal aquifer	France	10	0.6
Rhine delta	The Netherlands	120	19.6
Coastal aquifers	Suriname	57	12
Fraser delta	Canada	>7	21.5

A Holocene transgression as the source of the groundwater salinities is mentioned in the cited papers, with the exception of those indicated in bold, where the description indicates that a Holocene transgression could be the source of the salinity. The geographical location of the delta and coastal systems are given in Supplementary Fig. 5, which also give the references.

Modelling of saltwater leaching from aquitard sediments

The preservation of original porewater for up to 10 kyr in thick, unweathered lacustrine and marine clay deposits has been documented and was interpreted to be controlled by the thickness, the hydraulic properties of the clay and the hydraulic gradient across the aquitard[21,22]. To test this hypothesis, numerical groundwater modelling was undertaken to assess the flushing of marine porewater from an aquitard on a geologic timescale. Initially, the effect of variations of aquitard clay thickness and hydraulic conductivity, as well as the impact of the time after sediment deposition, were modelled conceptually in pseudo one dimension using the code

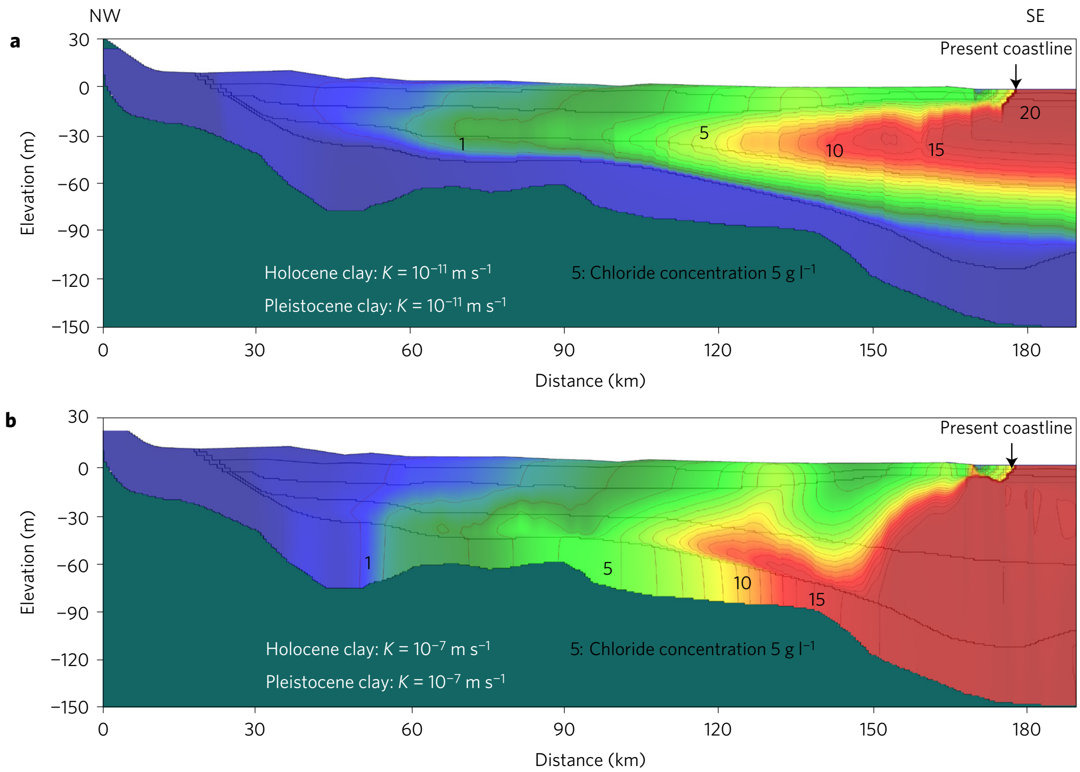

Figure 4 | Simulated salinity distributions in the RRDP sediments. a, Groundwater flow simulation of the present-day distribution of groundwater salinities in the RRDP, shown as porewater chloride concentrations. The hydraulic conductivity of the Holocene and Pleistocene clays in the simulations is 10^{-11} m s^{-1} (for further details, see Supplementary Information). **b**, Groundwater flow simulation of the present-day distribution of groundwater salinities in the RRDP, with a hydraulic conductivity which generates density-driven transport of marine porewater out of the Holocene clays (hydraulic conductivity of both the Holocene and Pleistocene clays of 10^{-7} m s^{-1}). For further information of the model set-up (see Supplementary Information).

SEAWAT (Supplementary Information and Flow Animation 1a–c). In the simulations, original marine porewaters are represented by a chloride concentration of 20 g l^{-1}. The simulations show that in clays with hydraulic conductivities of 10^{-8} m s^{-1} and lower, chloride concentrations after 6 ka are approximately 18 g l^{-1}, and 15 g l^{-1} after 11 ka. With a hydraulic conductivity of 10^{-7} m s^{-1}, the effect of density-driven transport is seen. With a hydraulic conductivity of the clay of 10^{-6} m s^{-1}, groundwater is fresh (<1 g l^{-1}) after a few hundred years. The relatively slow leaching of salty porewater from sediments with a hydraulic conductivity of 10^{-8} m s^{-1} or lower is explained by diffusion-controlled leaching of solutes out of the sediments, whereas a faster, density-driven transport is generated at higher hydraulic permeability in the aquitard clay[23].

The impact of the clay aquitard thickness on saltwater leaching by diffusion is shown in Supplementary Fig. 4. Simulated porewater compositions in the middle of the 60-m-thick clay are approximately 1–2 g l^{-1} after 60 ka, in clay with a 30 m thickness the porewater will be fresh after approximately 15 ka, and in clays with a thickness below 10 m, porewater will be fresh after a few hundred years. Based on these conceptualized, one-dimensional (1D) numerical models, salty porewater in 60-m-thick aquitard sediments ($K < 10^{-8}$ m s^{-1}) from the last interglacial period (Eemian; 130–120 ka) should now be replaced by freshwater, providing that the hydraulic properties of adjacent sediments permit transport out of the aquitard, and that saltwater has not subsequently been re-introduced. On the other hand, marine porewater should still be present in the Holocene marine aquitard clays.

2D hydrogeological models were constructed to assess saltwater leaching during the Holocene period (11 ka), based on the geology Fig. 2a. Modelling was done using eleven sub-models each of 1 kyr duration, in which the geologic sequence is progressively increased following the RRDP sedimentological model for the past 11 kyr (ref. 17). The model domain contains up to six geologic units as displayed in Fig. 2a. The Holocene clay (layer 4), the Holocene sand (layer 5), and the recent clayey soil (layer 6) are included in the sub-model simulations after deposition of these layers. A prescribed hydraulic head boundary was applied at the sea given by sea-level changes in the South China Sea during the past 11 kyr (ref. 17) (Fig. 1b). The palaeo-hydraulic gradients in the RRDP during the Quaternary period is not known, but must, as today, have been controlled by the palaeo-gradients of the land surface. A shallow, phreatic water table is in hydraulic contact with a dense network of channels, and the thickness of the unsaturated zone only up to few metres. A prescribed hydraulic head boundary was there also used inland, and was adjusted in every sub-model period to maintain a total horizontal hydraulic gradient of 0.3‰; a hydraulic gradient comparable to the present-day situation in the RRDP. However, in the flat part of the delta, the gradient is only approximately 0.05‰. Changing the total hydraulic gradient to 0.1‰ had a minor effect on the simulation result with respect to distribution of groundwater salinity (see Supplementary Information). Higher hydraulic gradients are physically impossible to develop during the Holocene period, as the surface water, and hence the land surface, is controlling the slope of the water table. A hydrostatic pressure distribution was applied at the coastlines in all sub-models. Using an initial chloride concentration of 20 g l^{-1} in both high- and low-permeability Pleistocene deposits did not lead to results comparable to present-day observed groundwater salinities in the RRDP. Therefore, the initial concentration of chloride in the Pleistocene sediment was set to 0.1 g l^{-1}, and from 2.0 g l^{-1}, inland, to 20.0 g l^{-1}, seaward, in the Holocene clay. The scenario with initially freshwater in the low-permeability Pleistocene deposits is supported by our conceptual 1D modelling, and freshwater conditions occurring in the high-permeability layers is in accordance with observations in

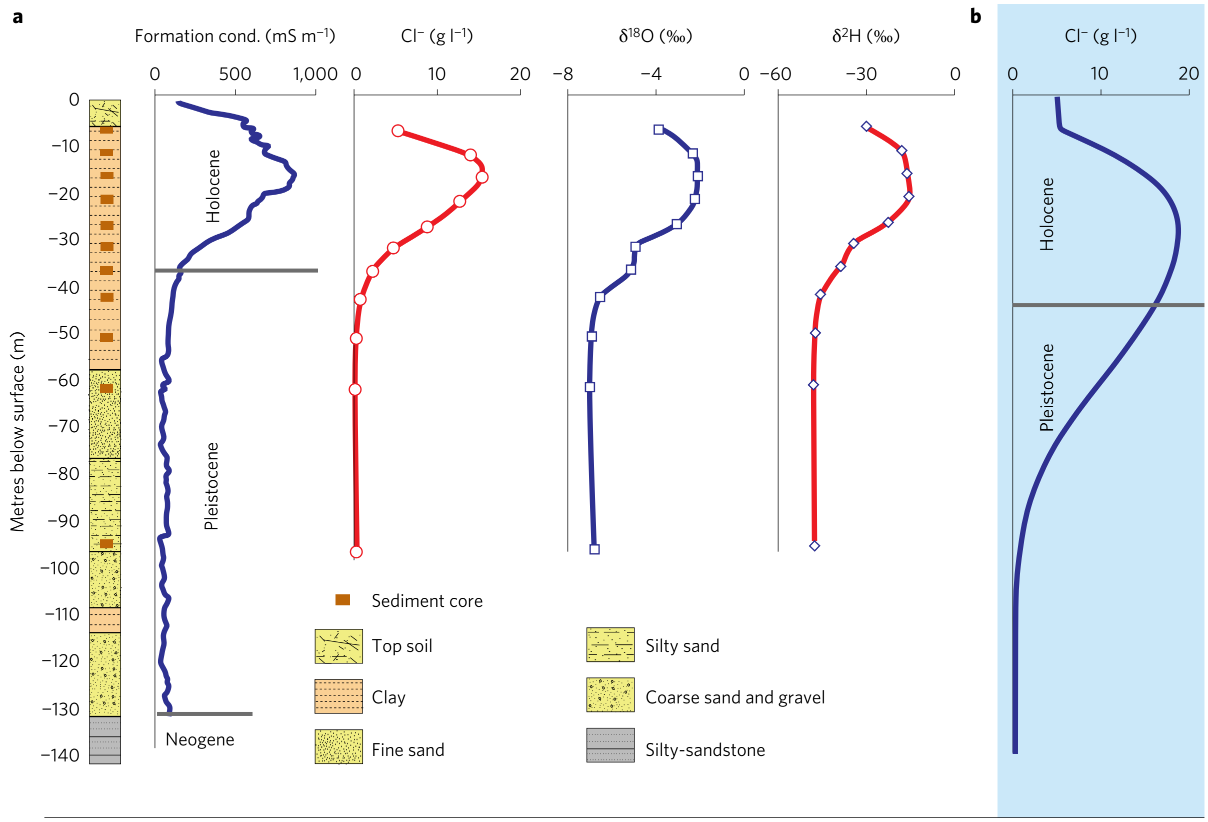

Figure 5 | Geology and water composition in exploratory borehole VA1. a, From left to right: the geologic composition of sediments, the formation conductivity measured with borehole geophysical logging, porewater chloride composition from cores, water-stable isotope compositions in porewater from cores and exported 2D modelling result. **b**, Simulated present-day chloride distribution eight kilometres from the present coastline. Data are extracted from the simulations shown in Fig. 4a.

present-day coastal aquifers, where submarine freshwater discharge is reported[24]. The variation of salinity in the Holocene clay reflects a gradual change in depositional environment from freshwater mires to swamps to fully marine clay[20]. Other model parameters are listed in the Supplementary Information.

Saltwater flushing from Holocene clay ($K = 10^{-11}$ m s^{-1}) during the past 11 kyr is shown in Flow Animation 2 (Supplementary Information). The simulated present-day chloride concentrations in the Holocene clay porewater (Fig. 4a) are close to marine water (15 to 20 g chloride/l) in a zone up to 40 km from the present coastline, and then gradually decrease to about 10 g chloride/l at a distance of 50–60 km from the coast. Simulated chloride concentrations in the Holocene clay are very similar to observed groundwater salinities as revealed from the exploratory borehole (Fig. 5a) and surface geophysical measurements (Fig. 2b). The observed peak values of 15 to 16 g l^{-1} are captured in the simulations (Fig. 5b), but at a greater depth, due to thicker Holocene clay layers, at the site of the simulation, which is 15 km from the borehole location. Observed water stable isotope composition close to marine water (Fig. 5b), confirms a marine origin of this water.

The simulated porewater chloride concentrations in the Pleistocene clay near the coastline are, however, higher than observations from borehole logging (Supplementary Fig. 1). This might be explained by an upward, advective freshwater flow through the Pleistocene clay, a process which is not included in the simulations, as a hydrostatic pressure gradient was applied in the simulations (Fig. 4a).

Increasing the hydraulic conductivity of the Holocene clays to 10^{-7} m s^{-1} does not significantly change the simulated present-day distribution of chloride, as the transport of chloride out of the Holocene marine clays is controlled by the hydraulic conductivity of the underlying low-permeability Pleistocene clay. Increasing the hydraulic conductivity of both the Holocene and Pleistocene clays to 10^{-7} m s^{-1} significantly changed the salinity distribution in the entire RRDP, and a distribution not resembling the present-day situation was obtained (Fig. 4b). The saltwater distribution with a uniform clay hydraulic conductivity of 10^{-7} m s^{-1} is caused by the onset of downward density-driven advective transport of the heavy salty groundwater in both the Holocene and Pleistocene clays, and an increasing horizontal seaward transport in the deep Pleistocene aquifer into the sea (see Flow Animation 3 in Supplementary Information). In the simulations, the transport of salty groundwater out of the RRDP reaches a Ghyben–Herzberg steady-state condition after approximately 5 kyr from today.

Broader impacts

Continental margin delta systems can be divided into shallow deltas (shelf-edge systems), formed during relatively small ($<\sim$150 m) eustatic sea-level changes, and deep-water deltas (shelf-delta systems) that accumulate under larger changes in the sea level[25,26]. Holocene deltas are typically shallow deltas in which high- and lowstand permeable sediments are connected, thereby creating a good hydraulic contact between coarse-grained shelf and continental deposits. Our simulations demonstrate that in coastal aquifers, the adjustment of groundwater chloride to rapid sea-level changes in thick, low-permeability aquitard sediments can take up to 40–50 kyr, and consequently the fresh–saltwater interface in Holocene deltas may be in a non-equilibrium state, depending on the thickness of the clays. Studies of the expansion and contraction in coastal groundwater systems, in response to the Quaternary changes in global sea level, have so far mainly been focused on the mode of seawater intrusion into existing geologic layers with variable permeability. Where the sea floods high-permeability layers, a relatively fast horizontal and vertical downward salinization will occur[27–29], whereas salinization of low-permeability muds and clays will be slow and dominated by diffusion[24,30]. We infer that another important salinity source in delta systems is the re-distribution of trapped saline water in marine aquitards. The slow diffusion-controlled transport of solutes out of clay layers, when the hydraulic conductivity of the layers is below 10^{-8} m s^{-1}, affects the quality of the groundwater in adjacent aquifers for thousands of years, causing these to become brackish or salty. Hydraulic heads in the shallow aquifers of Quaternary delta plains are controlled by the interaction with rivers, and are therefore close to sea level. Hydraulic head close to sea level is also present in deep aquifers near the sea, where groundwater is transported to the sea as a submarine groundwater discharge[24,31]. Consequently, the hydraulic gradients across aquitards in low-lying delta areas are typically small, which minimize advective flow through the deposits. A further complication regarding subsurface transport of water and dissolved solids in coastal zones is the occurrence of palaeo-channels in the sediments, as these can act as preferred pathways for water transport between aquifers and the sea[32]. However, as shown in this study, these palaeo-channels might also have been filled up with low-permeability, seawater-bearing sediments. Given the magnitude of the global sea-level changes in the Quaternary period[14], the thickness of sediments in palaeo-channels inland can be up to 100 m, and the implication is a long leaching period even on a geologic timescale.

The global sea level has been considerably lower than the present-day level for well over 90 % of the past 120 kyr (ref. 12), and in coastal zones that are not affected by major changes in subsidence rate and sediment supply, the main transgressive event is the Early Holocene transgression[12]. Based on observations and modelling results from this study, we suggest that where low-permeability marine deposits from the Holocene period are present in Quaternary delta systems, trapped palaeo-salty porewater will be confined to these clay layers, while saltwater in Pleistocene clay has now been leached out.

Methods

Methods, including statements of data availability and any associated accession codes and references, are available in the online version of this paper.

Received 17 October 2016; accepted 20 March 2017; published online 25 April 2017

References

1. Martínez, M. L. *et al*. The coasts of our world: Ecological, economic and social importance. *Ecol. Econ.* **63,** 254–272 (2007).
2. Small, C. & Nicholls, R. J. A global analysis of human settlement in coastal zones. *J. Coast. Res.* **19,** 584–599 (2003).
3. Chang, S. W. *et al*. Does sea-level rise have an impact on saltwater intrusion? *Adv. Wat. Resour.* **34,** 1283–1291 (2011).
4. Henry, H. Salt intrusion into fresh-water aquifers. *J. Geophys. Res.* **64,** 1911–1919 (1959).
5. Herzberg, B. Die Wasserversorgung einiger Norsseebäder. *J. Gasbeleuchtung Wasserversorggung* **44,** 815–819 (1901).
6. Reilly, T. E. & Goodman, A. S. Quantitative analysis of saltwater-freshwater relationships in groundwater systems - a historical perspective. *J. Hydrol.* **80,** 125–160 (1985).
7. Essink, G. H.P. O. Salt water intrusion in a three-dimensional groundwater system in The Netherlands: a numerical study. *Transp. Porous Media* **43,** 137–158 (2001).
8. Nguyen, A. D. *et al*. Using saltwater intrusion measurements to determine the freshwater discharge distribution over the branches of a multi-channel estuary: The Mekong delta case. *Estuar. Coast. Shelf Sci.* **77,** 433–445 (2008).
9. Wang, F. Dynamics of saltwater intrusion in coastal channels. *J. Geophys. Res.* **93,** 6937–6946 (1988).
10. Thanh, V. C. *Salinity Intrusion in the Red River Delta* (Department of Civil & Environmental Engineering, 1996); http://doi.org/10.2208/proer1988.22.213
11. Zhang, W. *et al*. Numerical simulation and analysis of saltwater intrusion lengths in the Pearl River delta, China. *J. Coast. Res.* **29,** 372–382 (2013).
12. Edmunds, W. M. in *Paleowaters in Coastal Europe: Evolution of Groundwater Since the Late Pleistocene* Vol. 189 (eds Edmunds, W. M. & Milne, C. J.) 1–16 (The Geological Society, 2001).
13. Shackleton, N. J. The 100,000-years ice-age cycle identified and found to lag temperature, carbon dioxide, and orbital eccentricity. *Science* **289,** 1897–1902 (2000).
14. Waelbroeck, C. *et al*. Sea-level and deep water temperature changes derived from benthic foraminifera isotopic records. *Quat. Sci. Rev.* **21,** 295–305 (2002).
15. Fisk, H. N. The loess and Quaternary geology of the lower Mississippi Valley. *J. Geol.* **59,** 333–356 (1952).
16. Rao, S. V. N. *et al*. Planning groundwater development in coastal deltas with Paleo channels. *Wat. Res. Manage.* **19,** 625–639 (2005).
17. Tanabe, S. *et al*. Holocene evolution of the Song Hong (Red River) delta system, northern Vietnam. *Sediment. Geol.* **187,** 29–61 (2006).
18. Tran, L. T. *et al*. Origin and extent of fresh groundwater, salty palaeowaters and recent saltwater intrusions in the Red River flood plain aquifers, Vietnam. *Hydrogeol. J.* **20,** 1295–1313 (2012).
19. Stanley, D. J. & Warne, A. Worldwide initiation of holocene marine deltas by deceleration of sea-level rise. *Science* **265,** 228–231 (1994).
20. Tran, N. *et al*. Quaternary sedimentation of the principal deltas of Vietnam. *J. Southeast Asian Earth Sci.* **6,** 103–110 (1991).
21. Remenda, V. H. *et al*. Isotopic composition of old ground water from Lake Agassiz: implications for late Pleistocene climate. *Science* **266,** 1975–1978 (1994).
22. Wang, Y. & Jio, J. J. Origin of groundwater salinity and hydrochemical processes in the confined Quaternary aquifer of the Pearl River delta, China. *J. Hydrol.* **438,** 112–124 (2012).
23. Groen, J. *et al*. Salinization processes in paleowaters in coastal sediments of Suriname: evidence from δ^{37}Cl analysis and diffusion modeling. *J. Hydrol.* **234,** 1–20 (2000).
24. Post, V. E. A. *et al*. Offshore fresh groundwater reserves as a global phenomenon. *Nature* **504,** 71–78 (2013).
25. Carter, R. M., Abbott, S. T., Fulthorpe, C. S., Haywick, D. W. & Henderson, R. A. in *Sedimentation, Tectonics and Eustasy: Sea-Level Changes at Active Margins* (ed. Macdonald, D. I. M.) Ch. 2 (Blackwell Publishing Ltd, 1991).
26. Postma, R. M. Two models: global sea-level change and sequence stratigraphic architecture. *Sediment. Geol.* **112,** 23–36 (1998).
27. Kooi, H. *et al*. Modes of seawater intrusion during transgressions. *Wat. Resour. Res.* **36,** 3581–3589 (2000).
28. Post, V. E. & Kooi, H. Rates of salinization by free convection in high-permeability sediments: insight from numerical modeling and application to Dutch coastal area. *Hydrogeol. J.* **11,** 549–559 (2003).
29. Delsman, J. R. *et al*. Paleo-modeling of coastal saltwater intrusion during the Holocene: an application to the Netherlands. *Hydrol. Earth Syst.* **18,** 3891–3905 (2014).
30. Bridger, D. W. & Allen, D. M. An investigation into effects of diffusion on salinity distribution beneath the Fraser delta, Canada. *Hydrogeol. J.* **14,** 1423–1442 (2006).
31. Kolker, A. S. *et al*. Pathways and processes associated with transport of groundwater in deltaic systems. *J. Hydrol.* **498,** 319–334 (2013).
32. Mulligan, A. E. *et al*. The role of paleochannels in groundwater/seawater exchange. *J. Hydrol.* **335,** 313–329 (2007).

Acknowledgements

The project received financial support as a research capacity building grant from the DANIDA research council (Grant 8-075-KU). P. T. K. Trang and her students from Hanoi University of Science are thanked for the chemical laboratory work and J. R. Ineson (GEUS) for linguistic support.

Author contributions

F.L. and N.Q.P. conceived the project. L.T.T. interpreted the geologic data. L.V.T., H.V.H. and L.T.T. carried out the geophysical field data. A.V.C. carried out the geophysical data processing and interpretation. L.T.T. estimated the effective diffusion coefficient of the sediments. L.V.T., N.Q.P. and F.L. did the hydrogeological modelling. F.L., L.T.T., H.V.H. and N.Q.P. analysed and interpreted the data. F.L. wrote the paper.

Additional information

Supplementary information is available in the online version of the paper. Reprints and permissions information is available online at www.nature.com/reprints. Publisher's note: Springer Nature remains neutral with regard to jurisdictional claims in published maps and institutional affiliations. Correspondence and requests for materials should be addressed to F.L.

Competing financial interests

The authors declare no competing financial interests.

Methods

Data from 83 monitoring boreholes in the Vietnamese National Groundwater Monitoring Network were used to establish a geologic model of the Quaternary deposits in the RRDP. Robertson Geologging equipment was used for geophysical borehole logging of 63 boreholes, and sediment natural gamma radiation and formation electrical conductivity were measured. Formation electrical conductivities were recorded from inside borehole polyvinyl chloride (PVC) casings using a focused induction probe, which has a formation penetration depth of approximately 5 m. Mapping of the spatial distribution of saltwater in the RRDP was performed using the transient electromagnetic method[33]. We used a PROTEM 47 (Geonics) with a 40 m by 40 m transmitter loop in a central loop configuration. Current levels of the transmitter were between 0.3 A and 3.0 A, producing a maximum magnetic moment of 4,800 Am^2, and the turn-off time for the current was 2.5 μs. This relatively short turn-off time, in combination with early time windows, allows for a proper description of the resistivity properties of the uppermost parts of the subsurface. The decay of the secondary magnetic field recorded by the receiver coil was sampled over three segments to handle the high dynamic range of the received signal. For each segment, measurements were made in 20 time windows (gates). Initial noise tests showed that the signal-noise level was very high in the study area. The initial TEM data processing—that is, editing of data and assignment of data uncertainties—was done utilizing the HGG-SiTEM/Semdi software[34]. Subsequently, the TEM data were inverted to obtain 1D resistivity models of the subsurface using a laterally constrained inversion (LCI) scheme[35]. The LCI approach links 1D resistivity models using a soft constraint on the layer resistivity and layer boundaries. The constraints can be seen as initial values for the expected geologic variations between soundings.

An exploratory borehole was drilled through the Quaternary deposits and into underlying Neogene deposits. Sediment samples for laboratory experiments were collected using a wireline piston coring device[36]. With the use of a porewater squeezing device[37], a high pressure (N_2) was applied to extract porewater from 22.0-cm-long, 4.8-cm-diameter sediment core samples. The amount of water from each core sample varied between 20 and 40 ml. Immediately after sampling, the porewater samples were filtered through Sartorius Minisart cellulose acetate filters (0.45 μm). Water samples for determination of stable isotopic composition were not filtered. Water samples were analysed as follows: water composition of Na, K, Ca and Mg were preserved with 2% of a 7 M HNO_3 solution and refrigerated until analysed by flame absorption spectrophotometry on a Shimadzu AAS 6800 instrument. Samples for Cl, NO_3 and SO_4 were collected in polypropylene vials and frozen immediately after sampling. The anions were analysed by ion chromatography using a Shimadzu LC20AD/HIC-20ASuper. Due to high salinities in the samples, up to 250-fold dilution was required. A 18 MΩ cm deionized water was used in the dilutions. Porewater stable isotope ratios of oxygen ($^{18}O/^{16}O$) and hydrogen (D) ($^{2}H/^{1}H$) were measured relative to the VSMOW (Vienna standard mean ocean water) standard using a Picarro cavity ring-down spectrometer (CRDS)[38] equipped with an autosampler and a vaporizer. The results are expressed in ‰ units using the δ-notation, with standard deviations not larger than ±0.2‰ ($\delta^{18}O$) and ± 0.5‰ (for δD), as calculated from four replicate injections into the vaporizer.

Effective diffusion coefficients of porewater constituents were determined in the laboratory by steady-state through-diffusion experiments and Holocene marine samples using a double-cell device[39]. A linear increase in mass indicates that a quasi-state diffusion prevails, and Fick's first law was used to express the diffusive flux though the samples[39].

Groundwater flow and solute transport was modelled using the USGS–SEAWAT version 4 (ref. 40) and the SWS Visual MODFLOW interface[40,41]. SEAWAT couples the two commonly used codes MODFLOW[42] and MT3DMS[43] with a variable density and viscosity package. Model set-up and input parameters in these simulations are described in Supplementary Information.

Code availability. The SEAWAT code is available from USGS: https://water.usgs.gov/ogw/seawat. The SiTEM/Semdi software is available from the Hydrogeophysics group at University of Aarhus: http://hgg.au.dk.

Data availability. The data that support findings of this study are available from the corresponding author upon request.

References

33. Mills, T. *et al*. Time-domain electromagnetic soundings for mapping sea-water intrusion in Monterey County, California. *Groundwater* **26,** 771–782 (1988).
34. Auken, E. *et al*. EMMA—a geophysical training and education tool for electromagnetic modeling and analysis. *J. Environ. Eng. Geophys.* **7,** 57–68 (2002).
35. Auken, E. *et al*. Piecewise 1D laterally constrained inversion of resistivity data. *Geophys. Prospect.* **53,** 497–506 (2005).
36. Zapico, M. M. *et al*. A wire-line piston core barrel for sampling cohesionless sand and gravel below the water-table. *Groundwater Monit. Remediat.* **7,** 74–82 (1987).
37. Reeburgh, W. S. An improved interstitial water sampler. *Limnol. Oceanogr.* **12,** 163–165 (1967).
38. Kerstel, E. R. T. in *Handbook of Stable Analytical Techniques* (ed. De Groot, P. A.) (Elsevier, 2004).
39. Bonnesen, E. P., Larsen, F., Sonnenborg, T. O., Klitten, K. & Stemmerik, L. Deep saltwater in Chalk of North-West Europe: origin, interface characteristics and development over geological time. *Hydrogeol. J.* **17,** 1643–1663 (2009).
40. Langevin, C. D., Thorne, D. T. Jr, Dausman, A. M., Sukop, M. C. & Guo, W. *SEAWAT Version 4: A Computer Program for Simulation of Multi-Species Solute and Heat Transport* Techniques and Methods Book 6, Vol. 39, Ch. A22 (US Department of the Interior, US Geological Survey, 2007).
41. Langevin, C. D. & Guo, W. MODFLOW/M3DMS-based simulation of variable-density ground water flow and transport. *Ground Wat.* **44,** 339–351 (2006).
42. McDonald, M. G. & Harbaugh, A. W. in *Techniques of Water-Resources Investigations of the United States Geological Survey* Chapter A1 (US Geological Survey, Department of the Interior, 1988).
43. Zheng, C. & Wang, P. P. *A Modular Three-Dimensional Multispecies Transport Model* (US Army Corps of Engineers, 1998).